Atmospheric mass loss and evolution of short-period exoplanets: the examples of CoRoT-7b and Kepler-10b

H. Kurokawa[1,2*] and L. Kaltenegger[2,3]

[1] *Tokyo Institute of Technology, 2-12-1 Ookayama, Meguro- ku, Tokyo 152-8551, Japan*
[2] *Max Planck Institut fuer Astronomie, Koenigstuhl 17, 69117, Heidelberg, Germany*
[3] *Harvard Smithsonian Center for Astrophysics, 60 Garden St., 02138 MA,Cambridge, USA*

16 June 2018

ABSTRACT
Short-period exoplanets potentially lose envelope masses during their evolution because of atmospheric escape caused by the intense XUV radiation from their host stars. We develop a combined model of atmospheric mass loss calculation and thermal evolution calculation of a planet to simulate its evolution and explore the dependences on the formation history of the planet. Thermal atmospheric escape as well as the Roche-lobe overflow contributes to mass loss. The maximum initial planetary model mass depends primarily on the assumed evolution model of the stellar XUV luminosity. We adapt the model to CoRoT-7b and Kepler-10b to explore the evolution of both planets and the maximum initial mass of these planets. We take the recent X-ray observation of CoRoT-7 into account and exploring the effect of different XUV evolution models on the planetary initial mass. Our calculations indicate that both hot super Earths could be remnants of Jupiter mass gas planets.

Key words: Planets and satellites: atmospheres - composition - individual(CoRoT-7b, Kepler-10b) - physical evolution - Stars: activity

1 INTRODUCTION

Hundreds of short-period exoplanets and candidates (KOIs) have been found by transit and radial velocity observations (Borucki et al. 2011; Batalha et al. 2012; Auvergne et al. 2009). Most of these planets are located closer to their host star than any planet in our Solar System. Short-period exoplanets might lose substantial mass during their evolution because of atmospheric escape caused by intense XUV radiation (X-ray and extreme UV) from their host stars (see e.g. Lammer et al. 2009).

As extreme cases, we focus on the evolution of the super Earths, CoRoT-7b (Léger et al. 2009) and Kepler-10b (Batalha et al. 2011), where both mass and radius are known. CoRoT-7b has a mass of 7.38 ± 0.34 $M_\oplus$ (Hatzes et al. 2011) and a radius of 1.58 ± 0.10 $R_\oplus$ (Bruntt et al. 2010). Kepler-10b has a mass of $4.56^{+1.17}_{-1.29}$ $M_\oplus$ and a radius of $1.416^{+0.033}_{-0.036}$ $R_\oplus$ (Batalha et al. 2011). These measured masses and radii are consistent with Earth-like rock and iron composition (see e.g. Wagner et al. 2011). Both CoRoT-7b and Kepler-10b orbit a G-type star and have short-period orbit, 0.0172 ± 0.00029 AU (Léger et al. 2009) and 0.01684 ± 0.00032 AU (Batalha et al. 2011), respectively, providing extremely hot environments.

The mass loss evolution of CoRoT-7b was explored in previous studies, with different results, two studies found that CoRoT-7b could be a remnant of a Jupiter-mass gas giant which experienced intense atmospheric mass loss (Valencia et al. 2010; Jackson et al. 2010). Another study found that CoRoT-7b would need to have formed as an initial rocky planet (Leitzinger et al. 2011). The difference found in these evolution studies is a result of the different evolution models postulated for the planet as well as different stellar XUV luminosity evolution used, one based on the *Sun in Time* project (Ribas et al. 2005) used in Valencia et al. (2010) and Jackson et al. (2010) versus an evolution model of soft X-ray luminosity (Penz et al. 2008) as scale for the total XUV luminosity used in Leitzinger et al. (2011). Recent observations of the X-ray luminosity of CoRoT-7 (Poppenhaeger et al. 2012) estimated the whole XUV luminosity to be 2.4×10^{29} erg s^{-1}, larger by an order of magnitude than the values 5.1×10^{28} erg s^{-1} (Ribas et al. 2005) and 2.1×10^{28} erg s^{-1} (Penz et al. 2008) estimated from XUV models for the assumed age of CoRoT-7 of 1.5 Gyr. Mass loss evolution of Kepler-10b indicates that Kepler-10b should have formed as a rocky planet (Leitzinger et al. 2011). Their models were based on XUV model by Penz et al. (2008).

In this paper, we explore the effect of different XUV models on mass loss history and evolution of a close-in

* E-mail: kurokawa@nagoya-u.jp

planet. We use CoRoT-7b and Kepler-10b as examples of two different close-in planetary environments, to investigate in which initial states both planets could have been as well as their evolution. Section 2 introduces our numerical models, section 3 presents, and section 4 discusses our results.

2   NUMERICAL MODELS

Our planet evolution model solves for atmospheric mass loss and thermal contraction simultaneously. Jupiter-like gas giant planets having solar composition envelopes on solid cores are assumed as an initial state. The planetary radius and the intrinsic luminosity are obtained with a structure calculation (see 2.1) for each time step. The thermal energy loss rate is calculated using the intrinsic luminosity and the atmospheric escape rate is calculated using the stellar XUV flux. The incoming XUV flux is derived from the evolution of the XUV luminosity model of the host stars (see 2.2).

2.1   Structure Calculation

We assume a spherically symmetric planet with a solar composition envelope and a rocky core. The rocky core is assumed to have the observed mass and radius values of the planet. The effect of the core radius evolution on the evolution of a planet is neglected. The atmospheric envelope is in hydrostatic equilibrium and is divided into an upper radiative equilibrium layer and a lower convective layer. The mass conservation equation and the hydrostatic equation (Eq. 1 and Eq. 2) are solved for the whole envelope,

$$\frac{\mathrm{d}\ln r}{\mathrm{d}M_r} = -\frac{1}{4\pi r^3 \rho}, \tag{1}$$

$$\frac{\mathrm{d}\ln p}{\mathrm{d}M_r} = -\frac{GM_r}{4\pi r^4 p}, \tag{2}$$

where, r is the distance from the center of the planet, M_r is the enclosed mass at the distance r, p is the pressure, ρ is the density, and G is the gravitational constant. To calculate the temperature structure, an analytic solution of the plane-parallel two-stream approximation (Guillot 2010) is used in the radiative equilibrium layer (Eq. 3),

$$T^4 = \frac{3T_{\mathrm{int}}^4}{4}\left(\frac{2}{3}+\tau\right) + \frac{3T_{\mathrm{irr}}^4}{4}f\left(\frac{2}{3}+\frac{1}{\gamma\sqrt{3}}+\left(\frac{\gamma}{\sqrt{3}}-\frac{1}{\gamma\sqrt{3}}\right)e^{-\gamma\tau\sqrt{3}}\right), \tag{3}$$

where T is the temperature, τ is the optical depth for outgoing long-wave radiation, T_{int} is the intrinsic temperature, T_{irr} is the irradiation temperature defined with the equilibrium temperature $T_{\mathrm{eq}} = f^{1/4}T_{\mathrm{irr}}$, f is the redistribution factor ($f = 1/4$ for full redistribution), and γ is the ratio of the short-wave to long-wave optical depth. We take $\gamma = 0.6\sqrt{T_{\mathrm{irr}}/2000\mathrm{K}}$ (following Guillot 2010), which provides a good match to detailed calculations of hot Jupiter atmospheres (Fortney et al. 2008). The intrinsic temperature T_{int} is defined by the intrinsic luminosity $L_{\mathrm{int}} = 4\pi R_{\mathrm{p}}^2\sigma_{\mathrm{SB}}T_{\mathrm{int}}^4$, where R_{p} is the planetary radius and σ_{SB} is the Stefan-Boltzmann constant. The optical depth τ is calculated using Eq. 4,

$$\frac{\mathrm{d}\ln\tau}{\mathrm{d}M_r} = -\frac{\kappa}{4\pi r^2\tau}, \tag{4}$$

where κ is the opacity for long-wave radiation. The plane-parallel approximation is only valid when the radiative equilibrium layer is thin compared to the planetary radius. This condition breaks down for highly irradiated atmospheres. Therefore we use the diffusion approximation equation (Rogers et al. 2011) (Eq. 5) for the lower part of the radiative equilibrium layer where incoming stellar radiation is not effective ($\tau \gg 1/\sqrt{3}\gamma$),

$$\frac{\mathrm{d}T}{\mathrm{d}r} = -\frac{3\kappa\rho}{16\sigma_{\mathrm{SB}}T^3}\frac{L_{\mathrm{int}}}{4\pi r^2}. \tag{5}$$

In the lower convective layer, an adiabatic temperature structure (Eq. 6) is assumed,

$$\frac{\mathrm{d}\ln T}{\mathrm{d}M_r} = -\frac{GM_r}{4\pi r^4 p}\left(\frac{\partial\ln T}{\partial\ln p}\right)_s, \tag{6}$$

where S is the entropy. The boundary between the radiative equilibrium layer and the convective equilibrium layer is determined by comparing the temperature lapse rate for a radiative equilibrium and an adiabatic lapse rate. We use the data table of Saumon et al. (1995) for the equation of state of solar composition gas and the Rosseland mean opacity data table of Freedman et al. (2008) for gas opacity. Out of the range of the opacity table, we use an power-law dependance Eq. 7 (following Rogers & Seager 2010),

$$\kappa = Cp^\alpha T^\beta, \tag{7}$$

where $\log C = -7.32$, $\alpha = 0.68$, $\beta = 0.45$ with all quantities in SI units. The upper boundary is defined as R_{p} at the layer where $\tau = 2/3$ and the pressure at the layer is obtained by Eq. 8,

$$\kappa p = \frac{2}{3}g, \tag{8}$$

where g is the gravity at the layer (following Rogers et al. 2011). The lower boundary is set to the radius of the core R_{core}. The equations are solved iteratively until a self-consistent structure for the assumed set of planetary mass M_{p}, core mass M_{core}, core radius R_{core}, irradiation temperature T_{irr}, and intrinsic temperature T_{int} is obtained. The observable planetary radius R_{p} is obtained as a result.

2.2   Evolution Calculation

Thermal evolution is calculated by integrating the energy equation (Eq. 9),

$$\int_{M_{\mathrm{core}}}^{M_p} T\frac{\mathrm{d}S}{\mathrm{d}t}\mathrm{d}M_r = -L_{\mathrm{int}}. \tag{9}$$

Here we neglect the contribution of the core because its thermal energy and radioactive energy is small compared to the energy of a massive envelope for giant planets. To integrate thermal evolution, entropy is assumed to be constant in the whole envelope, and to be the same as the entropy of the convective layer for simplification (see e.g. Valencia et al. 2010; Lopez et al. 2012). The thermal atmospheric mass loss is calculated by integrating the energy-limited escape rate formula (Eq. 10) (Lopez et al. 2012),

$$\frac{\mathrm{d}M_{\mathrm{p}}}{\mathrm{d}t} = \frac{\eta\pi F_{\mathrm{XUV}}R_{\mathrm{XUV}}^3}{GM_{\mathrm{p}}K_{\mathrm{tide}}}, \tag{10}$$

where η is the heating efficiency for which we use 25 % as the biggest estimate of mass loss (Leitzinger et al. 2011), F_{XUV} is the XUV flux, R_{XUV} is the distance from the center where the optical depth for XUV radiation equals unity, and K_{tide} is the correction factor that accounts for tidal effects in the Roche potential of planets (Erkaev et al. 2007) given by,

$$K_{\mathrm{tide}} = \left(1 - \frac{3}{2\xi} + \frac{1}{2\xi^3}\right), \tag{11}$$

$$\xi = \frac{R_{\mathrm{rl}}}{R_{\mathrm{XUV}}}. \tag{12}$$

The Roche-lobe radius, R_{rl}, is given by,

$$R_{\mathrm{rl}} = a_{\mathrm{p}}\left(\frac{M_{\mathrm{p}}}{3M_{\mathrm{star}}}\right)^{\frac{1}{3}}, \tag{13}$$

where a_{p} is the orbital distance from the host star and M_{star} is the mass of the star. R_{XUV} is calculated using Eq. 14 (Rogers et al. 2011),

$$R_{\mathrm{XUV}} = R_{\mathrm{p}} + H_{\mathrm{R}} \ln \frac{P_{\mathrm{R}} R_{\mathrm{XUV}}^2}{N_{\mathrm{H}} m_{\mathrm{H}} G M_{\mathrm{p}}}, \tag{14}$$

where, H_{R} is the scale height at $r = R_{\mathrm{p}}$, P_{R} is the pressure at $r = R_{\mathrm{p}}$, $N_{\mathrm{H}} \sim 10^{17}$ cm^{-2} is the column density of neutral hydrogen needed for the optical depth for XUV to equal unity, and m_{H} is the weight of a hydrogen atom.

The hydrodynamic wind is launched from the radius where the XUV radiation is absorbed. Therefore, we follow the model of Lopez et al. (2012) and use R_{XUV}^3 in the energy-limited escape rate formula (Eq. 10). Erkaev et al. (2007) used $R_{\mathrm{XUV}} \times R_{\mathrm{p}}^2$ instead of R_{XUV}^3. Valencia et al. (2010) and Leitzinger et al. (2011) used R_{p}^3 instead of R_{XUV}^3. To estimate the sensitivity of the results to this parameter, we calculate the difference of the escape rate as 40 % by setting $(R_{\mathrm{XUV}}/R_{\mathrm{p}})^3 \sim (17/15)^3 \sim 1.4$ (from our results in Fig. 4).

By integrating Eq. 9 and Eq. 10, we obtain M_{p} and the entropy of the convective layer for the next time step. Then a consistent structure is derived by solving the structure equations with T_{int} as input parameter.

The evolution model of stellar XUV luminosity which we use in this study dominates the mass loss calculation (Fig. 1) for close-in planets. Recent observations of the X-ray luminosity of CoRoT-7 (Poppenhaeger et al. 2012) estimated a total XUV luminosity of $L_{\mathrm{XUV}} = 2.4 \times 10^{29}$ erg s^{-1} for the star. For Kepler-10 there are currently no XUV observations available. Based on the observation of stellar XUV luminosity of G-type stars at different ages, Ribas et al. (2005) derived a scaling law (Eq. 15),

$$F_{\mathrm{XUV}} = 29.7\left(\frac{t}{1\mathrm{Gyr}}\right)^{-1.23} \text{ erg cm}^{-2}\text{ s}^{-1} \text{ at 1AU}, \tag{15}$$

where t is time. We use the XUV luminosity model in eq. 15 for Kepler-10. For CoRot-7, we assume the same power law but fix the absolute value to the measurement (Poppenhaeger et al. 2012). Because stellar XUV level is known to be constant for young star (e.g. Garcés et al. 2011), called the "saturation phase," we assume in our models that XUV luminosity is constant for the first 0.1 Gyr (following Valencia et al. 2010; Leitzinger et al. 2011). The sensitivity of the results to other XUV models are tested (see Discussion).
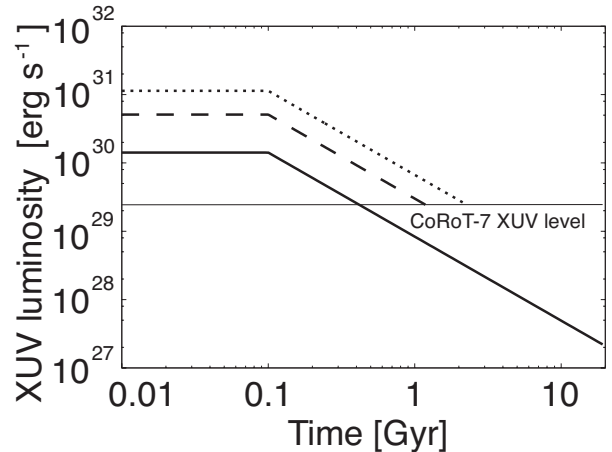

Figure 1. Evolution models of stellar XUV luminosity assumed in this work as a function of time. The solid line shows the scaling law of Ribas et al. (2005), assuming a saturation phase for the first 0.1 Gyr. The dashed and dotted lines show a similar model scaled to two different XUV flux observations for CoRoT-7 (Poppenhaeger et al. 2012).

The thermal atmospheric escape formula (Eq. 10) assumes that the Roche-lobe radius R_{rl} is larger than the XUV radius R_{XUV}. When R_{rl} becomes smaller than R_{XUV}, the upper atmosphere is no longer bound by planetary gravity. In that case, intense mass loss occurs until R_{rl} becomes larger than R_{XUV}. This mass loss mechanism is called *Roche-lobe overflow* and can be caused by orbital evolution (Gu et al. 2003; Jackson et al. 2010). In our models R_{XUV} becomes bigger than R_{pl} due to thermal atmospheric mass loss. When R_{rl} becomes smaller than R_{XUV}, we assume that the planet loses envelope mass rapidly until R_{rl} becomes larger than R_{XUV} without the thermal evolution by fixing the entropy of the convective layer. The assumption is justified because the timescale of the overflow is ~ 0.1 Myr (Gu et al. 2003) and is shorter than the time scale of thermal evolution and the age of the planets. Precise modeling of the overflow is beyond the scope of this paper.

3 RESULTS

Our assumption on the initial state of planets follows Valencia et al. (2010). To mimic the phase of planet formation and dissipation of the proto-planetary disk, planets are assumed to cool without atmospheric mass loss for the first 10 Myr. The lifetime of the disks is known to have diversity and 10 Myr is a longer estimate (Sicilia-Aguilar et al. 2006) that provides a conservative value for mass loss. We explore two formation scenarios, in situ formation and migration. In the migration scenario, planets are assumed to form at 0.1 AU, and migrate to their current orbit after the first 10 Myr. We neglect the period of the migration and thus planets migrate to their current orbit at the time of 10 Myr, conserving their entropy. We take the initial intrinsic luminosity $L_{\mathrm{int}} = 10^{-5} L_{\odot}$, as a typical value for young gas giant after the formation phase (Marley et al. 2007). The effect of
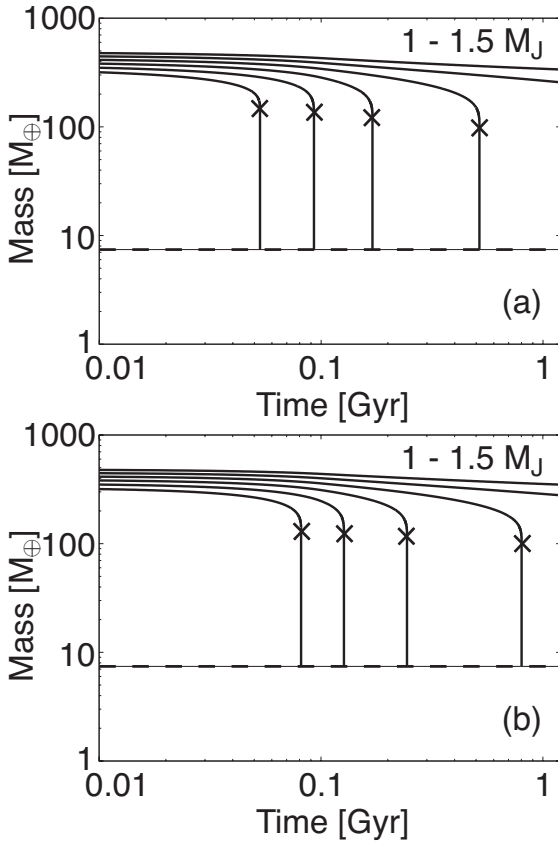
Figure 2. Evolution of the mass of hypothetical CoRoT-7b precursors as a function of time for an age of 1.2 Gyr and a core mass according to CoRoT-7b's 7.38 Earth masses indicated by the dashed line and initial total masses from 1.0 M_J to 1.5 M_J in steps of 0.1 M_J. Crosses indicate the time when Roche-lobe overflow occurs. Each panel shows the results of (a) in situ formation scenario, and, (b) migration scenario.

Figure 3. Evolution of the mass of hypothetical CoRoT-7b precursors as a function of time for an age of 2.3 Gyr and a core mass according to CoRoT-7b's 7.38 Earth masses indicated by the dashed line and initial total masses from 1.5 M_J to 2.0 M_J in steps of 0.1 M_J. Crosses indicate the time when Roche-lobe overflow occurs. Each panel shows the results of (a) in situ formation scenario, and, (b) migration scenario.

the initial luminosity on the mass loss evolution is discussed (see Discussion).

3.1   CoRoT-7b

For CoRoT-7b, we assume a core mass of $M_{core} = 7.38\ M_\oplus$, a core radius of $R_{core} = 1.58\ R_\oplus$, and an orbital distance of $a_p = 0.0172$ AU in accordance with the observed values. The effective temperature of CoRoT-7 is set to 5275 K (Léger et al. 2009). The age influences the stellar XUV flux model because its absolute current value is fixed to the measured value (Poppenhaeger et al. 2012). Because the age of CoRoT-7 is uncertain within 1.2 Gyr to 2.3 Gyr (Léger et al. 2009), we model both values.

The evolution of the mass of hypothetical CoRoT-7b precursors is shown in Figs. 2 and 3 which correspond to the results of the two different stellar ages. The maximum precursor masses which are consistent with CoRoT-7b's current mass are 1.3 M_J for a 1.2 Gyr stellar age model and 1.7 M_J for a 2.3 Gyr model.

In our models, Jupiter-mass precursors of both CoRoT-7b and Kepler-10b experience Roche-lobe overflow (shown as crosses in the figures) because of their small orbital distances from the host star. Fig. 4 shows a typical example of the
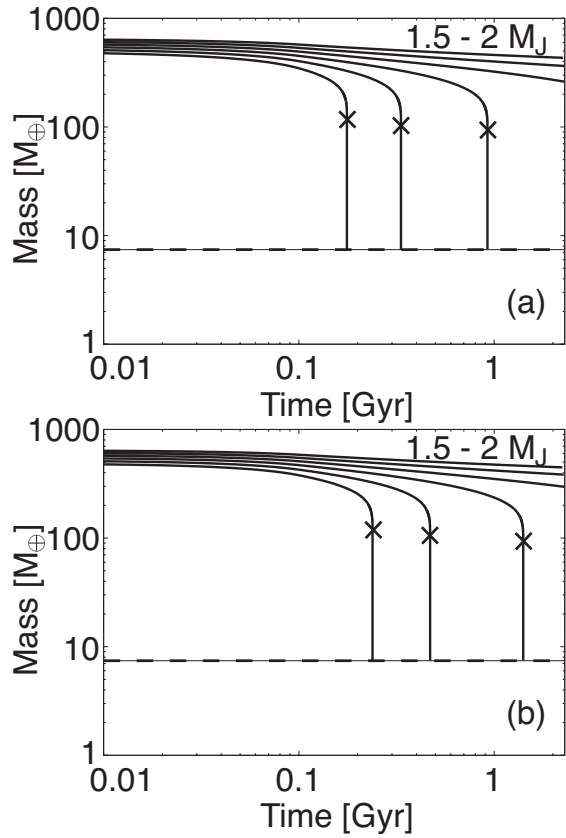
evolution of the planetary radius R_p, the XUV radius R_{XUV}, and the Roche-lobe radius R_{rl}. The mass loss caused by the thermal atmospheric escape decreases the Roche-lobe radius over the planet's evolution as well as increases the planetary radius before the overflow phase because of the decrease of planetary gravity. After the Roche-lobe overflow, the planet maintains only $\sim 0.01\ M_\oplus$ atmospheric mass and can loose the remaining atmosphere in a short time scale.

Slight differences of the initial mass result in large differences of the final planetary mass. This is because the thermal mass loss of the gas envelope decreases the density of the planets. It results in the increase of the mass loss rate (see Eq. 10). Roche-lobe overflow reduces the mass of the gas envelope even stronger. As a result, a difference of 0.1 M_J in initial mass can change the planet's evolutionary model from a super Earth which lost its whole envelope to a sub Jupiter planet which still maintains a massive envelope.

The different estimates of the age of CoRoT-7 changes the critical mass that can lose its whole envelope by $\sim$ 0.4 M_J because it changes the total value of the XUV luminosity received over the planet's evolution. The effect of the difference of the formation scenarios and respective distance where the planet initially formed on the critical mass is rather small $< 0.1\ M_J$ (not visible in Figs. 2 and 3 that
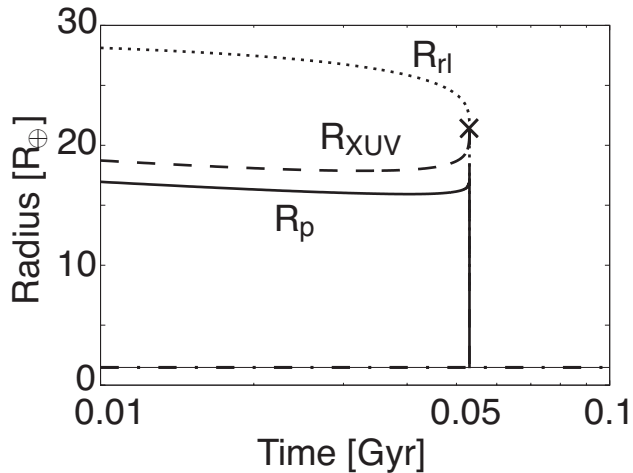
Figure 4. Example of the evolution of the planetary radius (solid line), the XUV radius (dashed line), and the Roche-lobe radius (dotted line) as a function of time, for the model of a CoRoT-7b precursor assuming in situ formation with an initial mass of 1.0 $M_{\rm J}$ and an age of 1.2 Gyr. The dash-dotted line is the assumed core radius. Crosses indicate the time when Roche-lobe overflow occurs.
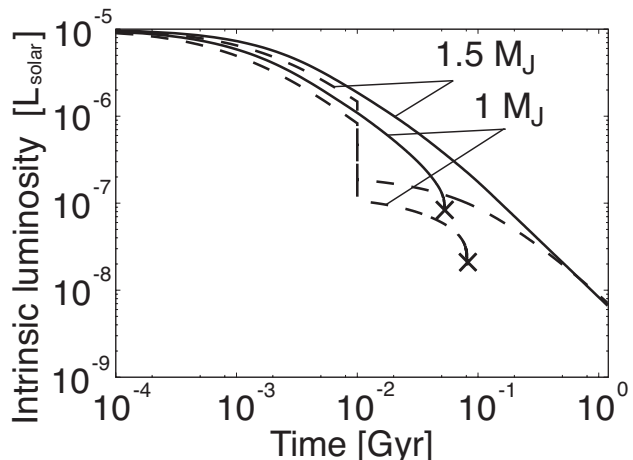

Figure 5. Examples of the evolution of the intrinsic luminosity for models of CoRoT-7b for an age of 1.2 Gyr. The solid lines and the dashed lines indicate the results for the case of in situ formation and migration respectively. The lower lines of the solid lines and the dotted lines which end at the Roche-lobe overflow points are the results of 1.0 $M_{\rm J}$. The upper lines are the results of 1.5 $M_{\rm J}$.

use a 0.1 $M_{\rm J}$ grid). This slight difference is caused by the difference in the initial radius of the planet. Migrated planets in our model have a smaller initial radius than planets which formed in situ, because a planet cools more efficiently when it is located in a cooler environment. The difference of the thermal states is shown by the intrinsic luminosities in Fig. 5.

3.2 Kepler-10b

For Kepler-10b, we assume a core mass of $M_{\rm core} = 4.56\ M_{\oplus}$, a core radius of $R_{\rm core} = 1.416\ R_{\oplus}$, and an orbital distance

of $a_{\rm p} = 0.01684$ AU, in accordance with observed values (Batalha et al. 2011). The effective temperature of the host star Kepler-10 is set to 5627 K. The estimated age of Kepler-10 is 11.9 ± 4.5 Gyr. We calculate the evolution of the hypothetical Kepler-10 precursors using a standard XUV luminosity model (Ribas et al. 2005). Therefore, the uncertainty of the age affects the total value of XUV received through the planet's evolution due to the lifetimes of the star but does not affect the absolute value of the XUV flux at each point of its evolution as in the case of CoRoT-7b.

The results are shown in Fig. 6. The maximum mass for Kepler-10b to be able to evolve from an initial gas giant planet into a rocky super Earth would be 1.1 $M_{\rm J}$. This indicates that a Jupiter mass gas giant planet could evolve into a super Earth like Kepler-10b through thermal atmospheric mass loss and Roche-lobe overflow. For Kepler-10b the maximum initial mass is smaller than that of CoRoT-7b because of the lower XUV flux level. Kepler-10b orbits a hotter host star and has a slightly smaller orbital distance than CoRoT-7b. The hotter environment makes atmospheric mass loss more intensive. However, the XUV luminosity has more dominant effect on the mass loss evolution and the lower XUV luminosity assumed for Kepler-10 results in the smaller maximum initial mass of Kepler-10b.

4 DISCUSSIONS

XUV flux dominates planetary mass loss. Here we summarize the effect of different stellar XUV flux evolution models (Fig. 7) and compare the results obtained. Ribas et al. (2005) investigated the XUV luminosity of six G type stars, including the Sun. The stars are nearby solar proxies whose rotation periods, temperatures, luminosities, and metallicities are well-determined. The range of the observed XUV is $1 - 1180$ Å. The data were obtained by an extrapolation for the range of $360 - 920$ Å where absorption by interstellar materials is strong. This model was used in our calculations. To quantify the sensitivity of our results to different stellar XUV evolution models, we apply different XUV models and calculate the evolution of Kepler-10b.

The model by Penz et al. (2008) is based on the mean X-ray luminosities of G-type stars in stellar clusters. They employed mean values motivated by the fact that the stellar X-ray luminosities vary by an order of magnitude. The work focused on X-ray luminosity ($1 - 200$ Å) because of the interstellar absorption of EUV. Garcés et al. (2011) collected the mean X-ray luminosities of G-, K-, and M-type stars in stellar clusters. Zuluaga et al. (2012) derived an evolution model of the stellar X-ray luminosity (Eq. 23 in their paper) based on the result of Garcés et al. (2011). The duration of the saturation phase is determined by connecting the two functions in Eq. 23 continuously.

Adopting the Penz et al. (2008) X-ray model for evolution models of Kepler-10b and maintaining the assumption of the 0.1 Gyr saturation phase (following Leitzinger et al. 2011) lead to a maximum mass loss of 0.8 $M_{\rm J}$ for Kepler-10b for in situ scenario and migration scenario, changing the maximum mass loss by -27 % for both scenarios. Adopting the Zuluaga et al. (2012) X-ray model, which has a ~ 0.04 Gyr saturation phase, leads to a maximum mass loss of 1.1 $M_{\rm J}$ for in situ formation and 1.0 $M_{\rm J}$ for mi-
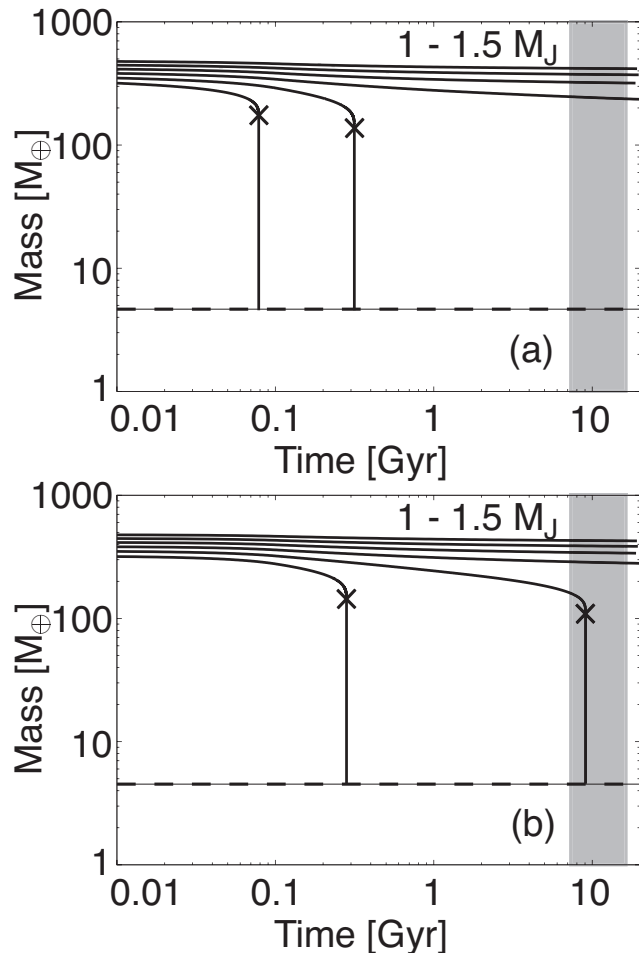
Figure 6. Evolution of the mass of hypothetical Kepler-10b precursors as a function of time for a core mass according to Kepler-10b's 4.56 Earth masses indicated by the dashed line and initial total masses from 1.0 M_J to 1.5 M_J in steps of 0.1 M_J. Crosses indicate the time when Roche-lobe overflow occurs. Each panel shows the results of (a) in situ formation scenario, and, (b) migration scenario. The range of the estimated age of Kepler-10b is shown by the gray zone.

Figure 7. Evolution models of stellar XUV (or X-ray) luminosity as a function of time: XUV scaling law of Ribas et al. (2005), assuming a saturation phase for the first 0.1 Gyr (solid line). X-ray scaling law of Penz et al. (2008), assuming a saturation phase for the first 0.1 Gyr (dashed line). X-ray scaling law of Zuluaga et al. (2012), based on the result of Garcés et al. (2011) (dotted line).

gration. These are changes of 0 % and −9.1 % for in situ formation and migration scenario respectively, comparing to our model. This analysis shows that the XUV evolution by Ribas et al (2005) provides a higher XUV environment and consequently higher planetary mass loss than models by Penz et al. (2008) and Zuluaga et al. (2012) because EUV is not included in their power laws. Note that our results should be used as upper limits on planetary mass loss for Kepler-10b and CoRoT-7b.

The mass loss evolution of CoRoT-7b and Kepler-10b has been studied by several previous works. Valencia et al. (2010) investigated the mass-loss evolution of CoRoT-7b and concluded that CoRoT-7b could be a remnant of a evaporated hot Jupiter. Jackson et al. (2010) studied the mass loss and the tidal evolution and concluded that the initial mass of CoRoT-7b does not exceed 200 Earth masses (2/3 Jupiter masses). The differences of our study from these works are the updated XUV model based on the observation of X-ray of CoRoT-7 and the mass-loss model which
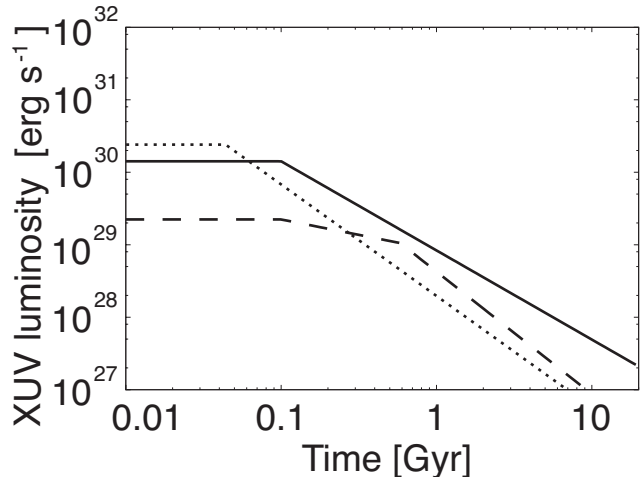
takes Roche-lobe overflow into account, both of which result in the enhanced mass-loss. The orbital evolution is not included our model. The thermal atmospheric escape and Roche-lobe overflow might affect the orbital evolution as well as the tide. Leitzinger et al. (2011) investigated the mass loss evolution of CoRoT-7b and Kepler-10b and concluded that these planets are not a remnant of a hot Jupiter. They used a scaling law for the evolution of the planetary radius. On the other hand, our model solves the evolution by calculating the structure of the planet consistently and finds different results.

In this paper, we use the energy-limited formula (Eq. 10) to calculate the thermal atmospheric escape, (following Valencia et al. 2010; Leitzinger et al. 2011). Thermal escape has a limiting mechanism, called the radiation-recombination limited escape, under extremely high XUV flux ($\sim 10^4$ erg cm^{-2} s^{-1}) condition (Murray-Clay et al. 2009). The radiation-recombination limit mechanism is caused by the thermostat effect of Lyα cooling. The XUV levels assumed in this work exceed that value in several cases. This limiting mechanism would decrease the thermal mass loss rate and reduce the initial maximum planetary mass obtained in our simulations. Exploring the effect on the planetary evolution is beyond the scope of this paper. In addition, non-thermal escapes such as the interaction with the stellar wind (e.g., Ekenbäck et al. 2010) can affect the total mass of the planet in the long term evolution.

In our calculation, $L_{\rm int} = 10^{-5} L_\odot$ is assumed for initial intrinsic luminosity. The effect of the initial intrinsic luminosity on the evolution can be understood by comparing the results of in situ formation and migration (Fig. 5). The intrinsic luminosity at 0.01 Gyr (the time of initial mass loss) differs by an order of magnitude between the two scenarios but affects the maximum initial planetary mass to evolve into a rocky super Earth only slightly (Figs. 2, 3, and 6).

5 SUMMARY AND CONCLUSION

CoRoT-7b and Kepler-10b are hot super Earths, with measured masses and radii, and have potentially experienced intense mass loss through their evolution caused by stellar XUV irradiation. We estimate the maximum mass of their initial planet by simulating the mass loss evolution of the hypothetical precursors using energy limited atmospheric escape and Roche-lobe overflow. The results show that both planets could be remnants of Jupiter mass gas planets. The conclusion is independent of the assumptions on evolution model of the stellar XUV luminosity and on formation scenarios. For such initial gas planets thermal atmospheric escape as well as Roche-lobe overflow determines the overall mass loss over the planet's evolution and its potential to evolve into a rocky super Earth in our model. This is because CoRoT-7b and Kepler-10b have small Roche-lobe radii caused by their small masses and small orbital distances from the host stars. The dependence on the formation scenario, which is interpreted as the difference of the intrinsic luminosity, is small. Our results show that mass loss for close in planets mainly depends on the stellar XUV flux. This model can also be applied to other known extrasolar planets.

REFERENCES

Auvergne, M., Bodin, P., Boisnard, L., et al. 2009, A&A, 506, 411

Batalha, N. M., Borucki, W. J., Bryson, S. T., et al. 2011, ApJ, 729, 27

Batalha, N. M., Rowe, J. F., Bryson, S. T., et al. 2012, arXiv:1202.5852

Borucki, W. J., Koch, D. G., Basri, G., et al. 2011, ApJ, 736, 19

Bruntt, H., Deleuil, M., Fridlund, M., et al. 2010, A&A, 519, A51

Ekenbäck, A., Holmström, M., Wurz, P., et al. 2010, ApJ, 709, 670

Erkaev, N. V., Kulikov, Y. N., Lammer, H., et al. 2007, A&A, 472, 329

Fortney, J. J., Lodders, K., Marley, M. S., & Freedman, R. S. 2008, ApJ, 678, 1419

Freedman, R. S., Marley, M. S., & Lodders, K. 2008, ApJs, 174, 504

Garcés, A., Catalán, S., & Ribas, I. 2011, A&A, 531, A7

Guillot, T. 2010, A&A, 520, A27

Gu, P.-G., Lin, D. N. C., & Bodenheimer, P. H. 2003, ApJ, 588, 509

Hatzes, A. P., Fridlund, M., Nachmani, G., et al. 2011, ApJ, 743, 75

Jackson, B., Miller, N., Barnes, R., et al. 2010, MNRAS, 407, 910

Lammer, H., Odert, P., Leitzinger, M., et al. 2009, A&A, 506, 399

Leitzinger, M., Odert, P., Kulikov, Y. N., et al. 2011, Planet. Space Sci., 59, 1472

Léger, A., Rouan, D., Schneider, J., et al. 2009, A&A, 506, 287

Lopez, E. D., Fortney, J. J., & Miller, N. 2012, ApJ, 761, 59

Marley, M. S., Fortney, J. J., Hubickyj, O., Bodenheimer, P., & Lissauer, J. J. 2007, ApJ, 655, 541

Murray-Clay, R. A., Chiang, E. I., & Murray, N. 2009, ApJ, 693, 23

Penz, T., Micela, G., & Lammer, H. 2008, A&A, 477, 309

Poppenhaeger, K., Czesla, S., Schröter, S., et al. 2012, A&A, 541, A26

Ribas, I., Guinan, E. F., Güdel, M., & Audard, M. 2005, ApJ, 622, 680

Rogers, L. A., & Seager, S. 2010, ApJ, 712, 974

Rogers, L. A., Bodenheimer, P., Lissauer, J. J., & Seager, S. 2011, ApJ, 738, 59

Saumon, D., Chabrier, G., & van Horn, H. M. 1995, ApJs, 99, 713

Sicilia-Aguilar, A., Hartmann, L., Calvet, N., et al. 2006, ApJ, 638, 897

Valencia, D., Ikoma, M., Guillot, T., & Nettelmann, N. 2010, A&A, 516, A20

Wagner, F. W., Sohl, F., Hussmann, H., Grott, M., & Rauer, H. 2011, Icarus, 214, 366

Zuluaga, J. I., Cuartas, P. A., & Hoyos, J. H. 2012, arXiv:1204.0275